Mechanics & Industry **23**, 25 (2022)
© B.-C. Yu and L.-S. Shao, Published by EDP Sciences 2022
https://doi.org/10.1051/meca/2022022

Mechanics & Industry

Available online at:
www.mechanics-industry.org

REGULAR ARTICLE

OPEN ACCESS

Optimization of the non-stop switchover system control for the main fans used in mining applications

Bao-Cai Yu* and Liang-Shan Shao

Institute of Systems Engineering, Liaoning Technical University, Liaoning 125105, China

Received: 4 May 2022 / Accepted: 29 June 2022

Abstract. A stable ventilation system is an essential guarantee for the efficient production and safety of underground workers. In order to solve the big changes in underground air quantity, gas accumulation, and other problems caused by mine main fans switchover. This paper proposes a non-stop switchover system of the mine main fans based on intelligent control and establishes a dynamic optimization model for the switchover process of the mine main fans. The equilibrium optimizer algorithm is improved by chaos mapping and opposition learning machine based on refraction principle to solve the model, and the simulation experiment is carried out with MATLAB. The results show that the proposed method can effectively mitigate the change of underground air quantity during the switchover process of mine main fans. In the 120 s of system operation, the change rate of underground air quantity is consistently within 0.4%, and the two mine main fans always work in the stable interval, which proves the system's high efficiency, stability and safety.

Keywords: Mine main fans switchover system / dynamic optimization model / equilibrium optimizer algorithm / chaotic mapping / opposition learning machine

1 Introduction

The essential function of the mine ventilation system is to provide fresh air for underground workers and equipment and to dilute harmful gases such as methane. In order to ensure the safety of underground workers, it is necessary to provide fresh air for underground workers continuously. According to relevant regulations, each return air shaft needs to install two sets of ventilation devices with the same capacity, one of them serves as a backup, and the main fan should be checked once a month. Thus the two main fans need to be rotated once a month. In most coal mine operations in China, the running fan is shut down first and then the backup fan is connected to the ventilation system. It is easy for mines with high gas concentrations to have gas accumulation during the mine main fans switchover period. If the backup fan fails, it will cause great danger to the underground mine and even cause serious accidents [1,2]. Therefore, the authors have proposed an intelligent control system to control the operating conditions of the two fans and the opening degree of the air doors so as to achieve the purpose of non-stop main fan switchover, minimize the fluctuation of underground air quantity and energy consumption [3,4].

Many experts and scholars put forward the constantly non-stop mine main fans switchover machine solution. Yu et al. [5] and Wu et al. [6] had proposed a non-stop mine main fans switchover scheme which has applied in most Chinese coal mines. Compared to the traditional way, the coal mine safety coefficient of ventilation system has been dramatically improved, and achieved the purpose of non-stop mine main fans switchover, but the air quantity fluctuation is still significant. Dong et al. [7] proposed an automatic control system based on fuzzy control, which significantly reduced the fluctuation of air volume. However, there are still risks for mines with high gas concentrations. Wang et al. [8] proposed the switchover model for the first time by combining the branch fluid dynamics and graph theory and developed an excitation control strategy according to the concept of fixed flow limiting. However, due to the complexity of the switchover model and the application of traditional algorithms, the operation speed is slow. Because the mine ventilation system is a complex system with high coupling and nonlinear characteristics, the above method will still cause the high fluctuation of underground air quantity, or the switching time will be too long, especially for some mines with high gas concentrations. The risk is still high and needs further improvement.

This paper proposes a no-stop mine main fans switchover system based on an improved equilibrium optimizer algorithm. This system can quickly find the

* e-mail: 1378425366@qq.com

This is an Open Access article distributed under the terms of the Creative Commons Attribution License (https://creativecommons.org/licenses/by/4.0), which permits unrestricted use, distribution, and reproduction in any medium, provided the original work is properly cited.

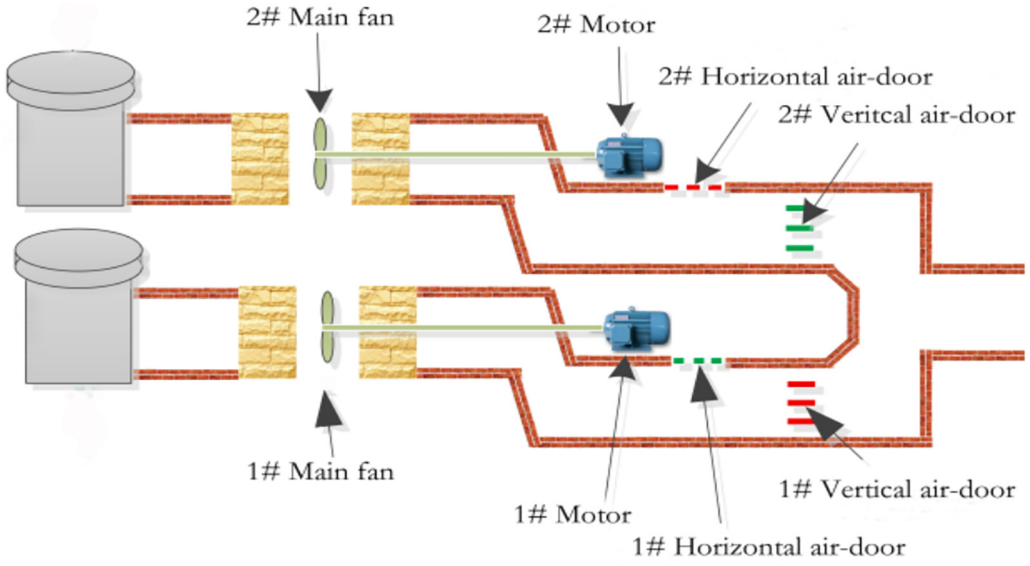

Fig. 1. Structure of mine main fans switchover system.

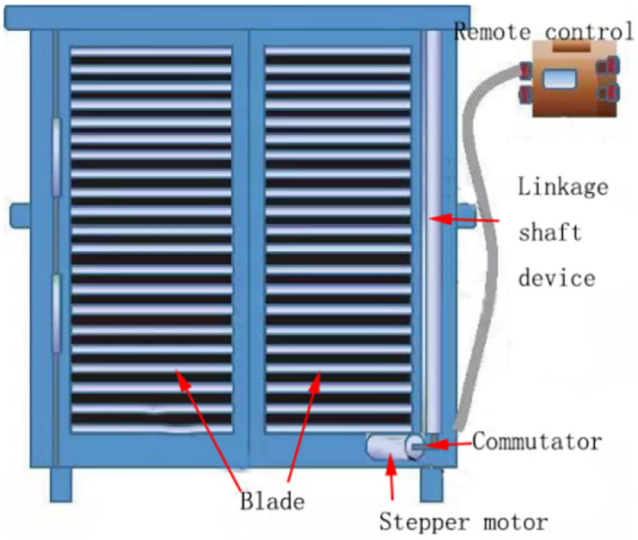

Fig. 2. Rotating vane type remote control air door.

best effective control scheme. By precisely controlling the opening and closing angles of the four air doors, it can achieve the goal of non-stop mine main fans switchover, constant underground air volume, and minimal energy consumption.

Figure 1 shows the structure of the mine main fans switchover system. It includes two main fans, one of them is a backup fan. Each fan has a horizontal air door and a vertical air door. The current working fan is 2# main fan. When the switchover command is issued, the 1# fan first starts to warm up. Then by controlling the four air doors, the 1# horizontal air door and 2# vertical air door gradually close. The 1# vertical air door and 2# horizontal air door gradually open simultaneously to ensure a constant underground air quantity.

In order to better adjust the angle of the air doors, this paper selects the fully automatic rotary vane air door. Figure 2 shows the structure diagram. The controller can accept instructions from the remote controller and transmit the instructions to the stepper motor. It can more accurately control the opening and closing angle of the four air doors to precisely control the air volume.

Figure 3 shows the schematic diagram of the no-stop switchover system of main mine fans based on intelligent control. When the switchover system starts operating, the optimized angle control instructions are transmitted to the PLC control cabinet through the control center, which controls the start and stop of the two main fan motors and the opening and closing angles of the four air doors blades. Then the sensor will collect the real-time angle of the air doors blade, air quantity and pressure. Furthermore, these signals are sent back to the control center cabinet through cable, which transmits the signal to the switching system to further adjust the throttle blade angle.

2 Modeling of mine main fans switchover system

2.1 Establishment of the equivalent model of the mine main fans switchover system

In order to facilitate the establishment of the mathematical model, the structural diagram shown in Figure 1 is simplified to the equivalent model shown in Figure 4, with a total of eight nodes, seven branches, and three virtual branches, where $M1$ and $M2$ represent two main fans branches, respectively. R_0 is the equivalent ventilation resistance in the underground mine (unit: $\mathrm{N}\cdot\mathrm{s}^2\cdot m^{-8}$). R_{1s} and R_{1c} are the equivalent ventilation resistance of 1# fan horizontal air door, 1# fan vertical air door, respectively (unit: $\mathrm{N}\cdot\mathrm{s}^2\cdot m^{-8}$). R_{2s} and R_{2c} are the equivalent ventilation resistance of 2# fan horizontal air door, 2# fan vertical air door, respectively (unit: $\mathrm{N}\cdot\mathrm{s}^2\cdot m^{-8}$). To study the fan switchover system's characteristics conveniently, it is approximately considered that the value of A is unchanged and the air in the roadway is not compressible. Node 1 represents the air inlet shaft, nodes

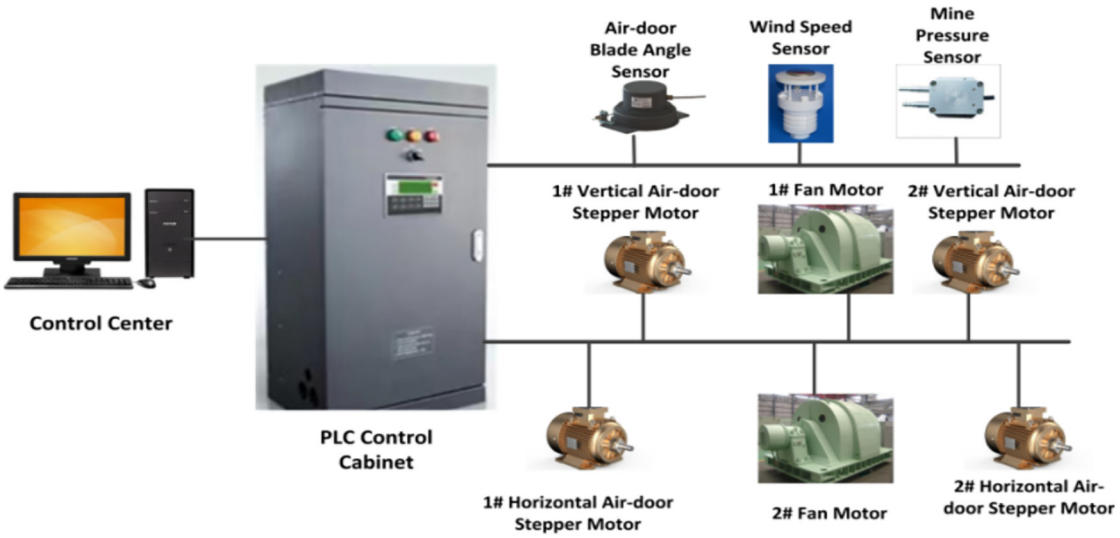

Fig. 3. Schematic diagram of the no-stop switchover system of main mine fans based on intelligent control.

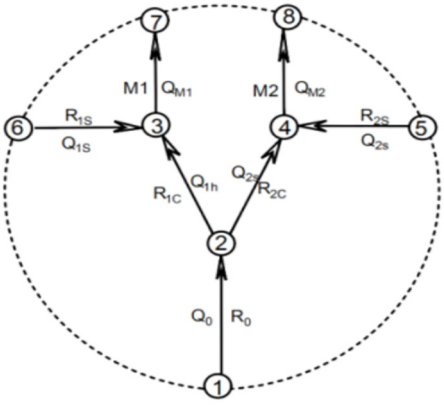

Fig. 4. Equivalent model of fan switchover system.

5 and 6 represent the outside of two horizontal air doors, and nodes 7 and 8 represent the two main fans' exhaust channels.

2.2 The characteristic of rotary blade air door

In order to reduce the change of underground air quantity during the mine main fans switchover process, this system selects the rotary blade air door. Therefore, the authors first study the relationship between the angle of the rotary blade air door and the ventilation resistance. The ventilation resistance of the rotary blade air door has a non-linear relationship with the blade angle. When the blade angle is 0°, the ventilation resistance is approximately 0, and the rotary blade air door is entirely open. When the angle is 90°, the ventilation resistance is close to infinity, and the rotary blade air door is entirely closed at this time. According to the conclusions of references [9,10], the approximate data of the ventilation resistance coefficient of the rotary blade air door τ and the blade angle $\theta°$ can be obtained. Table 1 is the corresponding ventilation resistance coefficient table.

The ventilation resistance of different types of rotary blade air door can be calculated according to equation (1). [20]

$$R = \frac{L}{S}\tau \ = [(M \times w)/2 \times (w + h)] \times \tau \tag{1}$$

where R is the equivalent ventilation resistance (unit: $\mathrm{N \cdot s^2 \cdot} m^{-8}$); L is the total length of the air door (unit: m) and S is the air door perimeter (unit: m), M is the number of blades in the rotary blade air door; w is the width of blade (unit: m); h is the height of the blade (unit: m).

Figure 5 is the fitting curve obtained by data. Using MATLAB to fit the data for five-degree polynomial [11,12], and get the expression as equation (2).

See equation (2) below.

Therefore, during the switchover period, the equivalent ventilation resistance of ith #fan at time t can be calculated according to equation (3)

$$R_{it} = \frac{R_{ist}(R_0 + R_{ict})}{R_0 + R_{ist} + R_{ict}} \quad i = 1, 2 \tag{3}$$

where R_{ist} and R_{ict} represent the equivalent ventilation resistance of the horizontal and vertical air doors of the ith #fan at time t, which can be obtained by entering the angle information transmitted by the air door angle sensor at time t into equation (2).

$$\tau = \begin{cases} 3.7266 \times 10^{-7} \times \theta^5 - 6.4747 \times 10^{-5} \times \theta^4 + 3.9429 \times 10^{-3} \times \theta^3 - 9559966 \times 10^{-2} \times \theta^2 + 0.78199 \times \theta - 0.15477, & 0° < \theta < 60° \\ 1.948 \times 10^{10} \times e^{-0.3902\theta} + 0.00164 \times e^{0.1245\theta} & 60° < \theta < 90° \end{cases}. \tag{2}$$

Table 1. The corresponding table of the ventilation resistance coefficient and the blade angle data of the rotary vane air door

Ventilation resistance coefficient τ	0.15	0.27	0.42	0.69	1.5	2.7	4.2	9.6	34.8	120
Blade angle $\theta(^\circ)$	0	10	20	30	40	50	60	70	80	90

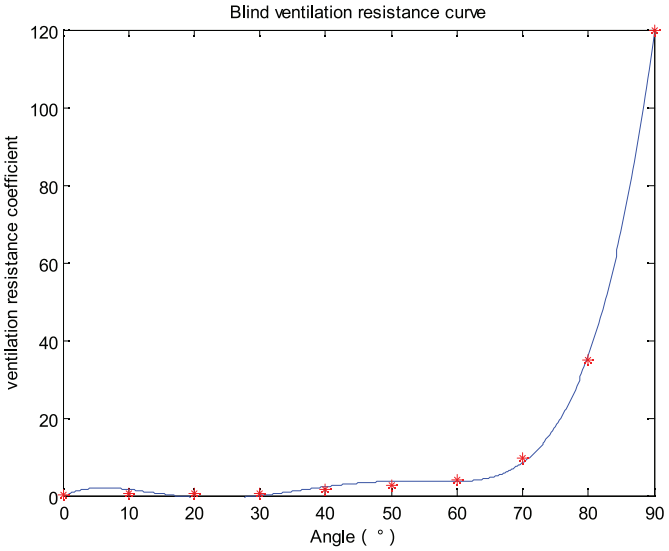

Fig. 5. Curve of ventilation resistance coefficient and blade angle of rotary blade air door.

Table 2. Performance parameter values converted to rated speed and standard ventilation state.

Q m^3/s	69.72	74.23	76.55	79.37	81.25	84.29	86.77
Total pressure/ Pa	2882.30	2901.45	2874.01	2811.53	2757.62	2640.61	2565.33

2.3 The characteristic of mine main fans

When modeling the mine main fans switchover system, the main fan characteristic curve data is very essential. The working condition of the fan can be assessed by combining the characteristic fan curve and the ventilation resistance characteristic curve [13], in order ensure that the two main fans have been working in a relatively safe and efficient state at time. Further research on the characteristic curves of the mine fans is required. As shown in Table 2, they are the performance parameters given in the test report at the Wang Jialing coal mine of Zhongmei Huajin Energy Co. Ltd. The parameters are converted to rated speed and standard ventilation state (dry air with the pressure of 760 mmHg and the temperature of 0 °C). This paper mainly studies the characteristics of air quantity and pressure, so only air quantity and pressure are given. According to the requirements of fan testing, the collected data shall be no less than six groups. The model of the fan is FBCDZ-8-NO28, which is an axial fan, and it is relatively common in mines.

In actual engineering, the most common method used in the curve fitting of ventilation turbines is the least-squares method of quadratic polynomial fitting. However, due to the significant deviation [14], the authors use a fourth-degree polynomial to fit the characteristic curve of the main fans. Figure 6 shows the curve after fitting the data in Table 2 with a fourth-degree polynomial. Surge phenomenon is prone to occur when the fan operating point is on the left side of point A. When it is working on the right side, the state is stable. The closer to point A, the higher efficiency. The intersection point B of the R_t line and the fan characteristic curve in the figure represent the fan operating point at time t.

According to the data in Table 2, fourth-degree polynomial fitting is performed with MATLAB to obtain relationship between the mine fan air quantity and pressure, as shown in equation (4)

$$H = -0.0002837Q^4 + 0.2022Q^3 - 53.99Q^2 + 6060Q - 2.507 \times 10^5. \quad (4)$$

2.4 The dynamic model of the main fans switchover system

When the switchover process is operating, the air flow diagram in the switchover system of the main fans is shown in Figure 3.

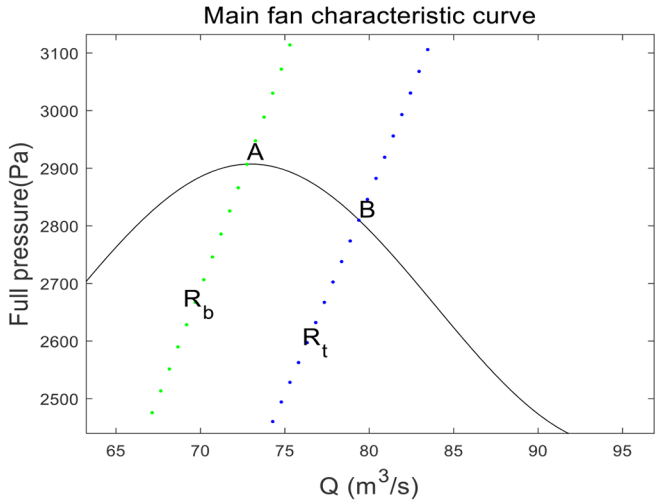

Fig. 6. Main fan air quantity-total pressure characteristic curve.

This modeling takes the minimum fluctuation of underground air quantity as the objective function, and the fluctuation of underground air quantity at time t can be expressed as equation (5).

$$\begin{aligned}\Delta Q_t &= Q_0 - Q_{0t} \\ &= Q_0 - (Q_{1ht} + Q_{2ht}) \\ &= Q_0 - ((Q_{1st} - Q_{M1t}) + (Q_{2st} - Q_{M2t}))\end{aligned} \tag{5}$$

where ΔQ_t refers to air flow fluctuation in underground at time t. Q_0 represents original air quantity in underground (unit m^3/s), Q_{0t} refers to air quantity in underground at time t (unit m^3/s), Q_{1ht} and Q_{1st} refer to air quantity through 1# vertical air door, 1# horizontal air door at time t, respectively (unit m^3/s), Q_{2ht} and Q_{2st} refer to air quantity through 2# vertical air door quantity, 2# horizontal air door at time t, respectively (unit m^3/s), Q_{M1t} and Q_{M2t} refer to air quantity through 1# main fan, 2# main fan at time t, respectively (unit m^3/s).

Since nodes 1, 5, 6, 7, and 8 are all exposed to the atmosphere, ignoring the influence of the position of the inlet and return air shafts, it is considered that the pressure of these nodes is equal to the atmospheric pressure, so it can be known that the pressure of the horizontal air door and the pressure of the fan at time t are equal, so it can be expressed by equations (6) and (7).

$$Q_{1st} = \sqrt{H_{1t}/R_{1st}} \tag{6}$$

$$Q_{2st} = \sqrt{H_{2t}/R_{2st}} \tag{7}$$

where H_{1t} and H_{2t} represents the pressure of the two main fans at time t, it is equal to the pressure through the horizontal air door, (unit Pa). It can be calculated by bringing the air quantity of the fan at time t into equation (4), as shown in equations (8) and (9), R_{1st} and R_{2st} represent the resistance of the horizontal air door at time t (unit $\mathrm{N}\cdot\mathrm{s}^2\cdot m^{-8}$). It can be calculated by substituting the data transmitted back through the damper angle sensor into equation (1).

$$\begin{aligned}H_{1t} = &-0.0002842Q_{M1t}4 + 0.2025Q_{M1t}3 \\ &- 53.15Q_{M1t}2 + 6065Q_{M1t} - 2.509 \times 10^5\end{aligned} \tag{8}$$

$$\begin{aligned}H_{2t} = &-0.0002842Q_{M2t}4 + 0.2025Q_{M2t}3 \\ &- 53.15Q_{M2t}2 + 6065Q_{M2t} - 2.509 \times 10^5.\end{aligned} \tag{9}$$

When the switchover process runs at time t, the horizontal air door, vertical air door and underground ventilation resistance are collectively regarded as an equivalent systems. The equivalent ventilation resistance R_{1t} and R_{2t} can be obtained by equation (3), as shown in equations (10) and (11). At this moment, the system satisfies the relationship of equations (12) and (13).

$$R_{1t} = \frac{R_{1st}(R_0 + R_{1ct})}{R_0 + R_{1st} + R_{1ct}} \tag{10}$$

$$R_{2t} = \frac{R_{2st}(R_0 + R_{2ct})}{R_0 + R_{2st} + R_{2ct}} \tag{11}$$

$$H_{1t} = R_{1t}Q_{M1t}^2 \tag{12}$$

$$H_{2t} = R_{2t}Q_{M2t}^2. \tag{13}$$

Combining equations (8)–(13), respectively, the Q_{M1t} and Q_{M2t} expressions can be obtained as equations (14) and (15).

$$Q_{M1t} = (14.43 - 9.18 \times 10^{-41}i)R_{1t} \tag{14}$$

$$Q_{M2t} = (14.43 - 9.18 \times 10^{-41})iR_{2t}. \tag{15}$$

Therefore, to express it more clearly, the equation (1) is rewritten as shown in equation (16). Substituting equations (1), (6), (7), (14), (15) into equation (5), finally equation (17) is obtained, where θ_1, θ_2, θ_3, θ_4 present the angles of the horizontal air door and vertical air door blades of 1# main fan and the angles of the horizontal air door and vertical air door blades of the 2# main fan at the time t, respectively.

$$R = \xi \times \tau \tag{16}$$

$$\begin{aligned}\Delta Q_t &= Q_0 - \left(\sqrt{\frac{H_{1t}}{\theta_1\xi}} + \sqrt{\frac{H_{2t}}{\theta_2\xi}}\right) \\ &= Q_0 - \left\{\begin{array}{l}(14.43 - 9.18 \times 10^{-41}i)\dfrac{\theta_1\xi(R_0 + \theta_3\xi)}{\theta_1\xi + R_0 + \theta_3\xi} \\ \\ + (14.43 - 9.18 \times 10^{-41}i)\dfrac{\theta_2\xi(R_0 + \theta_4\xi)}{\theta_2\xi + R_0 + \theta_4\xi}\end{array}\right\}\end{aligned} \tag{17}$$

After the transformation, the objective function is shown in equation (18).

See equation (18) below.

In order to ensure the safe and reliable operation of the main fans switchover system, the actual working ventilation pressure cannot be over 90% of the maximum pressure, and the switchover time cannot be over 10 min. According to the actual situation, the adjustment angle range of the four air doors is 0–90°, Due to the gear accuracy of the air door stepper motor, the adjustment angle of each step must be bigger than 0.1°. In summary, the constraint can be expressed as equation (19)

$$\begin{cases} R_{it} < R_A \quad i = 1,2 \\ H_{it} < 0.9H_{\max} \quad i = 1,2 \\ \theta_j \in [0^\circ - 90^\circ] \quad j = 1,2,3,4 \\ \triangle\theta > 0.1^\circ \end{cases}. \tag{19}$$

3 Equilibrium optimizer

3.1 Inspiration

The EO was introduced in 2019 by Faramaezi et al. [15]. The inspiration for the EO approach is a simple well-mixed dynamic mass balance on a control volume, in which a mass balance equation is used to describe the concentration of a nonreactive constituent in a control volume as a function of its various source and sink mechanisms. A generic mass balance equation can be described by a first-order differential equation, as shown in equation (20).

$$V\frac{dC}{dt} = QC_{eq} - QC + G \tag{20}$$

where V represents the control volume, C represents the concentration of particles in the control volume, $V\frac{dC}{dt}$ represents the rate of change in mass in the control volume, Q represents the volumetric flow rate into and out of the control volume, C_{eq} is the concentration of particles inside the control volume at an equilibrium state without generation and G is the mass generation rate inside the control volume. When $V\frac{dC}{dt} = 0$, a steady equilibrium state is reached. $\lambda = \frac{Q}{V}$ is defined in the paper as the turnover rate, where $\frac{Q}{V}$ is the inverse of the residence time. The equation (20) is rearranged as follows:

$$\frac{dC}{\lambda C_{eq} - \lambda C + \frac{G}{V}} = dt \tag{21}$$

Equation (22) shows the integration of equation (21) over time.

$$\int_{C_0}^{C} \frac{dC}{\lambda C_{eq} - \lambda C + \frac{G}{V}} = \int_{t_0}^{t} dt. \tag{22}$$

The result is show in equation (23)

$$C = C_{eq} + (C_0 - C_{eq})F + \frac{G}{\lambda V}(1 - F) \tag{23}$$

where F can be calculated using equation (24)

$$F = \exp\left(-\lambda(t - t_0)\right) \tag{24}$$

where t_0 and C_0 represent the initial time and concentration.

3.3 Equilibrium pool and candidates

The EO algorithm constructs a vector called the equilibrium pool [16,17], which provides equilibrium candidate particles. Five candidate particles of the equilibrium pool are determined by experiments, four of which are the optimal particles identified in the whole optimization process, and the other one is the arithmetic mean of the above four particles. Four optimal particles help to explore the search space better, while the average helps in exploitation. The vector of the equilibrium pool is as follows:

$$\vec{C}_{eq,pool} = \left\{\vec{C}_{eq(1)}, \vec{C}_{eq(2)}, \vec{C}_{eq(3)}, \vec{C}_{eq(4)}, \vec{C}_{eq(ave)}\right\}. \tag{25}$$

3.3 Exponential term *F*

Exponential term F[18] plays an important role in balancing the exploration and exploitation of the EO algorithm. The calculation is as follows:

$$F = e^{(-\lambda(t-t_0))} \tag{26}$$

where λ is a random vector between [0,1], t is an iterative function that decreases with the number of iterations. The calculation is as follows:

$$t = (1 - \frac{Iter}{Max_{iter}})^{\alpha_2 \frac{Iter}{Max_{iter}}} \tag{27}$$

where $Iter$ and Max_{iter} represent the current and the maximum number of iterations, respectively. The calculation of t_0 in equation (27) is as follows:

$$\vec{t}_0 = 1\vec{\lambda}\ln(-\alpha_1 sign(\vec{r} - 0.5)[1 - e^{-\lambda t}]) + t \tag{28}$$

$$\begin{aligned} \min W &= f(\theta_1, \theta_2, \theta_3, \theta_4) \\ &= \sum_{t=0}^{T} \triangle Q_t \\ &= \sum_{t=0}^{T} Q_0 - \left(\sqrt{\frac{H_{1t}}{\theta_1\xi}} + \sqrt{\frac{H_{2t}}{\theta_2\xi}}\right) \\ &= \sum_{t=0}^{T} Q_0 - \left\{(14.43 - 9.18 \times 10^{-41} i)\frac{\theta_1\xi(R_0 + \theta_3\xi)}{\theta_1\xi + R_0 + \theta_3\xi} + (14.43 - 9.18 \times 10^{-41} i)\frac{\theta_2\xi(R_0 + \theta_4\xi)}{\theta_2\xi + R_0 + \theta_4\xi}\right\} \end{aligned}. \tag{18}$$

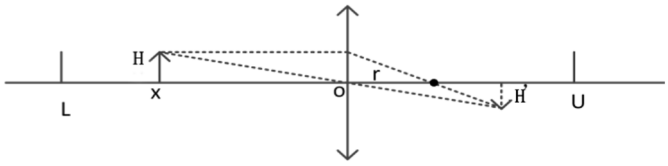

Fig. 7. Schematic diagram of lens imaging.

where α_1 and α_2 are constant, and they control exploration and exploitation capabilities, respectively. The higher the value of α_1, the stronger the exploration capability is and the worse the exploitation capability. The higher the value of α_2, the stronger the exploitation capability is and the worse the exploration capability. α_1 and α_2 are equal to 2 and 1, respectively. $\text{sign}(\vec{r}-0.5)$ indicates the direction of exploration and exploitation. Rearrange as equation (29).

$$\vec{F} = \alpha_1 \, sign(\vec{r}-0.5)[e^{-\vec{\lambda}\tau}-1]. \tag{29}$$

3.4 Generation rate *G*

Generation rate G guarantees the EO algorithm to provide accurate solutions by improving the exploitation capability. Assuming a first-order exponential decay process to define the generation rate [19,20], the calculation of G is as equation (30).

$$\vec{G} = \vec{G}_0 e^{-k(\vec{t}-t_0)} \tag{30}$$

where $\vec{G}_0$ is the initial value; k is a decay constant equal to $\vec{\lambda}$. Therefore, the final expression of the generation rate $\vec{G}_0$ is as equation (31), which equal to $\vec{\lambda}$. Therefore, the final expression of the generation rate $\vec{G}_0$ is as equation (32).

$$\vec{G} = \vec{G}_0 e^{-\vec{k}(t-t_0)} = \vec{G}_0 \vec{F} \tag{31}$$

where

$$\vec{G}_0 = GC\vec{P}(\vec{C}_{eq} - \vec{\lambda}\vec{C}) \tag{32}$$

$$G\vec{C}P = \begin{cases} 0.5r_1, & r_2 \geq GP \\ 0, & r_2 < GP \end{cases} \tag{33}$$

where r_1 and r_2 are random numbers between [0,1], and $G\vec{C}P$ indicates the probability that the generation term contributes to the updating process, which is called the generation rate control parameter; the probability of this contribution specifies how many particles use generation terms to update their state. $G\vec{C}P$ is obtained by equation (33), where is called the generation probability, and its role is to achieve a good balance between exploration and exploitation. Finally, the updating rule of EO is as follows:

$$\vec{C} = \frac{\vec{C}_{eq} + (\vec{C}_0 - \vec{C}_{eq})\vec{F} + \vec{G}}{\vec{\lambda}V(1-\vec{F})} \tag{34}$$

where V is considered a unit.

4 Proposed opposition based on chaotic map equilibrium optimizer (OB-C-EO)

4.1 Chaotic map

In the population iterative optimization algorithm, the size and range of the initial population have a significant impact on the quality of the solution and the speed of convergence. Since the location and concentration of the optimal solution are unknown at the beginning of the search, if the individuals of the initial population can be evenly distributed in the search space, it will effectively improve the search efficiency. In order to get a better initial value of diversity, the chaotic mapping algorithm is used to initialize the population.

Logistic mapping is a straightforward chaotic mapping in mathematical form. This system has extremely complex dynamics and has a wide range of applications. Its mathematical expression is as equation (35).

$$x_i^{k+1} = |1 - 2(x_i^k)^2| \tag{35}$$

where $x_i^k \in [0,1]$ is the chaotic sequence: $k = 1, 2, \ldots, L$, L is the initial population dimension: $i = 1, 2, \ldots, N$, N is the initial population number. Performing the mapping operation to x_i^k obtains the initial population y_i^k of the solution space, and the calculation is as shown in equation (36).

$$y_i^k = L_i + (U_i - L_i)x_i^k \tag{36}$$

where L_i and U_i are the boundary of the variable value.

4.2 Opposite learning mechanism based on the principle of refraction

Meta-heuristic algorithms generally have a slow convergence process and require multiple iterations to get the best solution. In order to prevent the algorithm from falling into the local optimum prematurely and speed up the convergence speed. In the search process, not only the usual solution, but also its opposite solution must be considered.

Therefore, this paper introduces the opposite learning mechanism based on the principle of refraction [21] into the algorithm. The process of finding the opposite point in the search space is described as follows: using the principle of light refraction to calculate, taking a certain dimension variable x_i as an example. The search interval range is $[l_i, u_i]$, the base point position is set as $(l_i + u_i)/2$, as shown in Figure 7, the height of the object located at x is H, and the height of the image at the location x' is H' after being refracted by the lens. According to the physical principle of lens imaging, the following equations can be obtained.

Table 3. Algorithm name and parameter setting.

Algorithm	Parameter	Value
PSO	Topology	Fully connected
	Cognitive and social constants	C1 = 2, c2 = 2
	Inertial weight	Linearly decreases from 0.9 to 0.4
WHO	Crossover percentage	PC = 0.13
	Stallions percentage (number of groups)	PS = 0.2
	Crossover	Mean
SSA	Lead position update probability	0.5
GA	Type	Real coded
	Selection	Roulette wheel
	Crossover	Single point 0.8
	Mutation	0.3
EO	$a1$	2
	$a2$	1
	GP	0.5
OB-C-EO	$a1$	2
	$a2$	1
	GP	0.5
	ρ	2

$$\frac{\frac{(l_i+u_i)}{2}-x}{x'-\frac{(l_i+u_i)}{2}}=\frac{H}{H'} \tag{37}$$

$$\frac{r}{x'-\frac{(l_i+u_i)}{2}-r}=\frac{H}{H'} \tag{38}$$

where r represents the focal length in the process of refraction. In the opposite learning mechanism, $\frac{H}{H'}$ represents the reverse search radius and the zoom factor, which is expressed by ρ. Combining equations (37) and equation (38) can get the calculation formula of the reversal point x'.

$$x'=\frac{1+\frac{1}{\rho}}{r}+\frac{l_i+u_i}{2} \tag{39}$$

where the focal length r can be calculated by equation (40).

$$r=\frac{l_i+u_i-2x}{2(\rho+1)}. \tag{40}$$

By adjusting the zoom factor and the reverse search radius, the purpose of controlling the distance and direction of the particle search is achieved. In the iterative process of the equilibrium optimizer algorithm, the zoom factor gradually decreases to the minimum as the number of iterations increases. The calculation equation is as follow.

$$\rho_i=\rho_{\max}-\frac{\rho_{\max}-\rho_{\min}}{T}i \tag{41}$$

where T represents the maximum number of the iterations.

$$r_i=r_{org}\bullet rand \tag{42}$$

where r_{org} represents the initial value, calculated by equation (40): *rand* is a random number in the range of [0,1].

After introducing the opposite learning machine based on the principle of refraction, the update equation of the equilibrium optimizer algorithm is shown in equation (43).

$$C_i(Iter)=\frac{2}{\rho_i\bullet\left[(li+ui)-2C_{eq}(Iter)\right]}. \tag{43}$$

The computational steps of the proposed improved equilibrium optimizer algorithm are described as pseudo-code in Appendix A.

5 Simulation experiment and analysis

5.1 Experiment related settings

The experimental environment is Windows10, 64 bit operating system, CPU is Inter Core i9-11950h, main frequency is 5.0 GHz, memory is 16GB. The algorithm program is written based on Matlab2020b. We will compare with other algorithms. Table 3 records the full name and abbreviation of the algorithm and its parameter settings.

Simulation experiments are carried out on 13 benchmark functions. Table 4 shows the details of the test functions. Among them, functions F1–F7 are unimodal functions, and there is only one global optimal meridian, suing to evaluate the convergence speed of the algorithm.

Table 4. Benchmark function.

Function	Dim	Range	Fmin
$F_1(x) = \sum_{i=1}^{n} x_i^2$	30	[–100, 100]	0
$F_2(x) = \sum_{k=1}^{n} \lvert x_i \rvert + \prod_{k=1}^{n} \lvert x_i \rvert$	30	[–10,10]	0
$F_3(x) = \sum_{i=1}^{n} (\sum_{j=1}^{i} x_j)^2$	30	[–100,100]	0
$F_4(x) = \max_j \{ \lvert x_i, 1 \le i \le n \}$	30	[–100,100]	0
$F_5 = \sum_{i=1}^{n-1} [100(x_{i+1} - x_i^2)^2 + (x_i - 1)^2]$	30	[–30,30]	0
$F_6(x) = \sum_{i=1}^{n} ([x_i + 0.5])^2$	30	[–100,100]	0
$F_7(x) = \sum_{i=1}^{n} i x_i^4 + \text{random}[0,1]$	30	[–1.28,1.28]	0
$F_8(x) = \sum_{i=1}^{n} - x_i \sin(\sqrt{\lvert x_i \rvert})$	30	[–500,500]	0
$F_9(x) = \sum_{i=1}^{n} [x_i^2 - 10\cos(2\pi x_i) + 10]$	30	[–1.25,1.25]	0
$F_{10}(x) = -20\exp\left\{-0.2\sqrt{\frac{1}{n}\sum_{i=1}^{n} x_i^2}\right\} - \exp(\frac{1}{n}\sum_{i=1}^{n}\cos(2\pi_{x_1})) + 20 + e$	30	[–32,32]	0
$F_{11}(x) = \frac{1}{4000}\sum_{i=1}^{n} x_1^2 - \prod_{i=1}^{n}\cos(\frac{x_1}{\sqrt{t}}) + 1$	30	[–600,600]	0
$F_{12}(x) = \frac{\pi}{n}\left\{10\sin(\pi y_1) + \sum_{i=1}^{n-1}(y_i - 1)^2[1 + 10\sin^2(\pi y_{i+1})] + (y_n - 1)^2\right\} + \sum_{i=1}^{n} u(x_i, 10, 100, 4)$ $y_i = 1 + \frac{x_i + 1}{4}$ $u(x,a,k,m) = \begin{cases} k(x,-a)^m & x_i > a \\ 0 & -a < x_i < a \\ k(-x,-a)^m & x_i < -a \end{cases}$	30	[–50,50]	0
$F_{13}(x) = 0.1\{\sin^2(3\pi x_1) + \sum_{i=1}^{n}(x_i - 1)^2[1 + \sin^2(3\pi_i + 1)] + (x_n - 1)^2[1 + \sin^2(2\pi x_n)]\} + \sum_{i=1}^{n} u(x_i, 5, 100, 4)$	30	[–50,50]	0

Table 5. Experimental comparison results.

F		GA	PSO	WHO	SSA	EO	OB-C-EO
F_1	Avg	3.1480E–07	1.2550E–05	7.8960E–01	2.2560E–13	4.3356E–28	**1.5689E–45**
	Std	2.1610E–07	4.5350E–05	1.2258E+00	1.2500E–16	2.2580E–28	**7.2500E–30**
F_2	Avg	1.6325E+00	1.1250E–02	1.5380E–02	3.2560E–02	7.7690E–16	**6.2500E–23**
	Std	1.2502E+00	4.5860E–02	2.3430E–01	8.9760E–01	1.5280E–15	**0.0000E+00**
F_3	Avg	7.1594E+02	6.5254E+01	5.6116E+02	5.9652E+02	2.2350E–05	**1.5500E–17**
	Std	1.3892E+04	8.8125E+01	2.0157E+02	2.3893E+02	4.5890E–04	**8.8900E–12**
F_4	Avg	1.2651E+01	3.1250E+00	1.5800E–01	5.0026E+00	3.6580E–06	**7.6800E–14**
	Std	3.2782E+00	1.2540E–01	6.8970E–01	5.6380E–01	1.1570E–05	**7.8650E–11**
F_5	Avg	2.5006E+01	1.0122E+02	5.8813E+02	1.2356E+02	**1.8123E+01**	2.2257E+01
	Std	5.0324E+01	6.5288E+01	2.2810E+02	2.2519E+02	7.3560E–01	1.0036E+01
F_6	Avg	2.3800E–05	1.2589E–05	4.2110E–01	**2.2250E–14**	8.8490E–01	7.8250E–01
	Std	3.2560E–05	3.3591E–05	1.6071E+00	7.8780E–16	**7.7520E–01**	4.3850E–07
F_7	Avg	2.2430E–01	2.7240E–02	3.2230E–02	8.5312E–02	**5.6380E–03**	1.2250E–02
	Std	1.4530E–01	8.0400E–03	1.5940E–02	2.2590E–02	8.1250E–02	**3.8500E–03**
F_8	Avg	–5.2151E+03	–5.0358E+03	**–1.5428E+04**	–1.7536E+03	–5.5763E+03	–9.8893E+03
	Std	7.6226E+02	7.5613E+02	2.1411E+02	3.5600E+02	8.8953E+02	5.6823E+02
F_9	Avg	5.6202E+01	4.2352E+01	2.0119E+01	2.7856E+00	5.6780E–01	**7.0071E–54**
	Std	5.0023E+01	6.7261E+00	6.5723E+00	5.5534E+00	4.8390E–01	**5.6890E–43**
F_{10}	Avg	1.4521E+00	5.0210E–03	2.0056E+00	1.2350E–02	5.6860E–12	**2.2256E–13**
	Std	2.2530E–02	5.2570E–02	3.3690E–01	7.8450E–01	2.2400E–13	**3.6954E–13**
F_{11}	Avg	5.5100E–04	5.6880E–02	4.8790E–01	2.2103E+01	4.4800E–03	**7.9700E–07**
	Std	4.5830E–03	3.5600E–02	1.3890E–01	2.0239E+00	6.6500E–03	**7.6900E–07**
F_{12}	Avg	6.8735E+00	4.5280E–02	1.2560E–01	8.9980E–01	5.3430E–02	**0.0000E+00**
	Std	3.4258E+00	5.5480E–02	5.6100E–02	2.8370E–01	2.0730E–02	**0.0000E+00**
F_{13}	Avg	1.2126E+01	6.1200E–03	4.4350E–01	2.8021E+00	1.2380E–01	**2.2130E–03**
	Std	2.1145E+01	2.5000E–03	5.5980E–01	6.2536E+00	1.2700E–04	**6.5980E–07**

Functions F8–F13 are a multimodal test function used to evaluate the algorithm performance in avoiding local optimization and exploration.

5.2 Experimental results and analysis

In order to prove the effectiveness and robustness of the proposed OB-C-EO, we compare the OB-C-EO algorithm with PSO [22], WHO [23], SSA [24], GA [25], EO [15]. At the same time, the population number of all algorithms is 30 and the maximum number of iterations is 500. All algorithms run independently on 13 benchmark functions 50 times and take the average and standard deviation of 50 times as the final evaluation index. Table 5 shows the specific experimental data. Where Ave represents the average optimal fitness value, Std represents the standard deviation, we bold the best result.

We can know from Table 5, no matter in unimodal functions or multimodal function, put forward the improvement of balance optimizer algorithm performance is superior to other algorithms, it is because of the initial particle by chaotic mapping on optimization, and the introduction of learning mechanism of opposites, can enhance the ability of particle escape from local optimum, to enhance the searching capability of the algorithm.

5.3 Convergence analysis

Figure 8 shows the convergence evaluation results of OB-C-EO and the comparison algorithm in Table 1 in different functions. In order to facilitate observation, the ordinate value is logarithm base 10. From the figure, we can know that the convergence speed of the proposed improved equilibrium optimizer algorithm is faster than other algorithms in both the exploration and exploitation stage. Its search accuracy is better than other algorithms. Such a result cannot be separated from the introduced improved strategy. Combined with Table 6, we can know that the improved equalization optimizer algorithm proposed has fast convergence speed and high optimization accuracy in both single-peak and multi-peak functions.

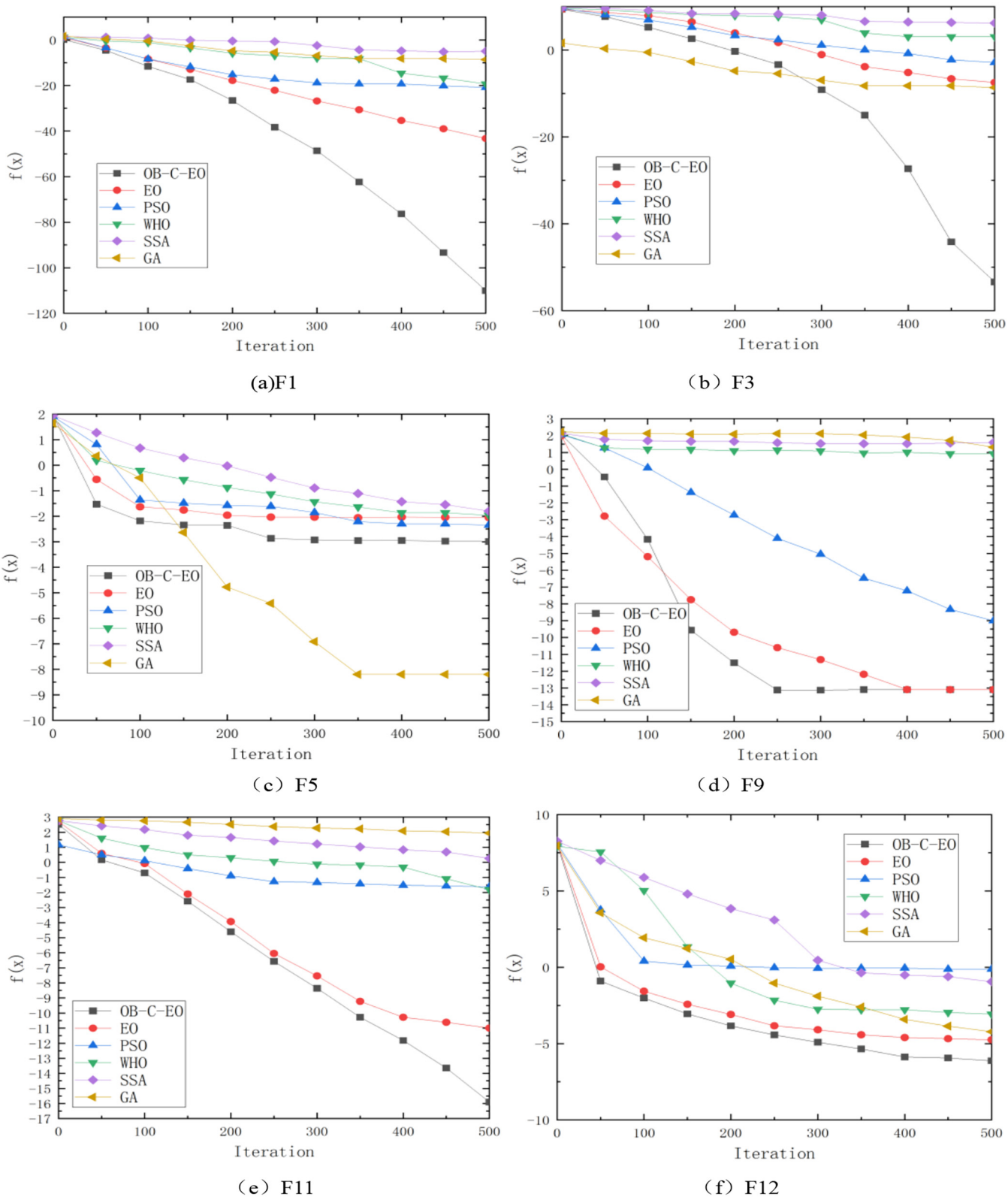

Fig. 8. Average convergence curve.

Table 6. Simulation parameter settings.

M Number of blades	8
W Blade width	0.3 m
H Blade height	1.8 m
R_0	0.16 $N \cdot s^2 \cdot m^{-8}$
Q_0	74.3 m^3/s
θ_3	12°

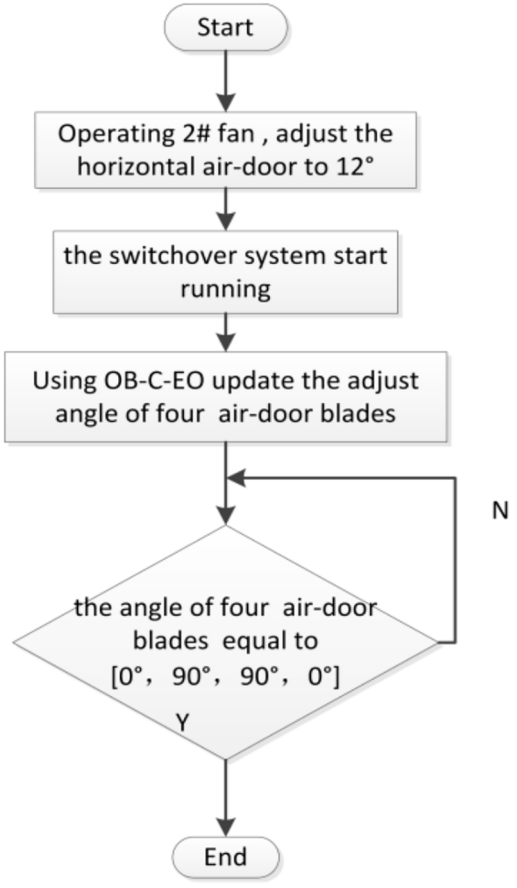

Fig. 9. The flowchart for switchover system.

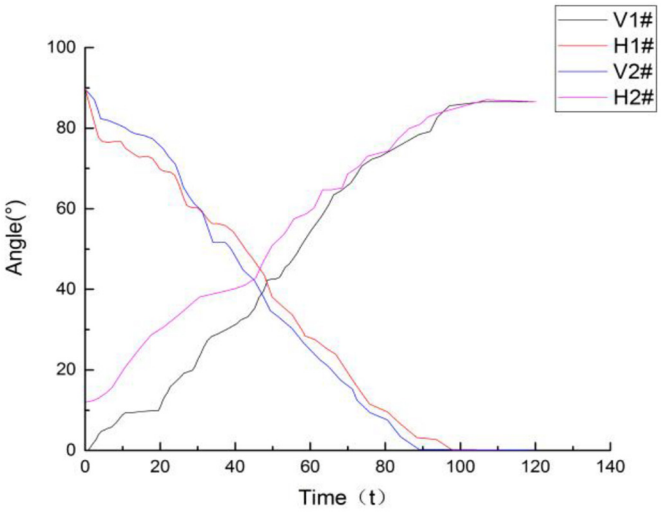

Fig. 10. Angle changes of four rotary blade air door.

6 Engineering experiment analysis

6.1 Simulation settings

According to the above discussion, in the main fans switchover system, each adjustment of the four air doors blinds is a non-linear optimization. Therefore, the penalty function is used to transform equation (18) into the fitness function, as shown in equation (44)

$$\text{Fitness} = |f(\theta_1, \theta_2, \theta_3, \theta_4)| + o_1 \sum_{i=1}^{2} (\ln R_{it}) + o_2 \sum_{i=1}^{4} (\ln \theta_{it}) \quad (44)$$

where o_1 and o_2 are the penalty function coefficients. According to the constraint optimization model of the mine main fans switchover system established by Formula (19), the improved equalization optimizer algorithm is applied to solve the problem. The simulation is carried out in MATLAB. Table 6 shows the simulation parameter settings. The algorithm parameters are the same as those in Section 5.1.

Before the simulation starts, operate the 2# fan is operated and the angle of θ_3 is adjusted, to make the state of 2# fan close to the operating point of the 1# fan. At this time, the 2# fan is entirely opened and operated normally. The switchover process starts to run and gradually adjusts $\theta_1, \theta_2, \theta_3, \theta_4$ make these angles change from [90°, 12°, 0°, 90°] to [0°, 90°, 90°, 0°]. When the angles of the four air doors reach [90°, 0°, 0°, 90°], the 1# fan is entirely off the network and in the no-load state. The 1# fan can be shut down and the 2# fan can be kept as the working fan. Now the switchover process is completed. The flowchart for the process is demonstrated in Figure 9.

6.2 Simulation result analysis

The system operating time is 120 s. Figure 10 shows the angle changes of the four rotary blade air doors during switching.

Figure 11 shows the underground air quantity change rate with the adjustment of the four rotary blade air doors. The underground air quantity change rate can be obtained by dividing ΔQ_t (obtained from Eq. (5)) by Q_0, during the adjustment process, Q_t may be less than Q_0, so there will be a negative value. It can be seen from this figure that since the equivalent ventilation resistance of the air door varies significantly with the blade rotation at the beginning of adjustment, the air flow quantity fluctuates wildly. With the system operating, the underground air quantity

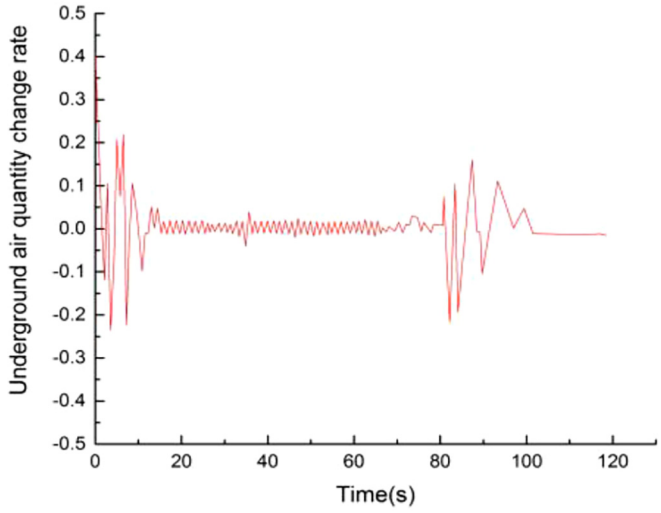

Fig. 11. Underground air quantity change rate.

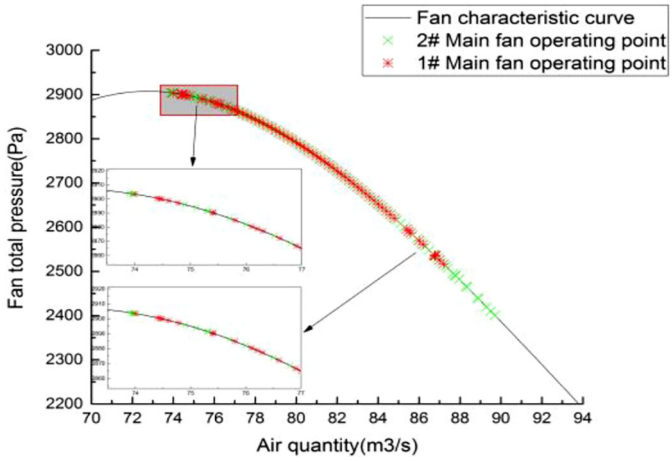

Fig. 12. Variation of operating points of two main fans during switchover operation.

fluctuation gradually stabilizes. In the later stage of the system operation, the equivalent ventilation resistance of the air door changes significantly, which causes the air quantity fluctuations in the second half of the system operation. After about 100 s, the system gradually stabilizes. After 120 s, the entire switchover process is completed. It can be seen from Figure 11 that during the operation of the system, the change rate of underground air quantity does not exceed 0.4%, which is greatly improved compared with the references [26,27], in which the change rate of underground air quantity is 8.1% and 5%.

Figure 12 shows the changes of the operating point of the two main fans during the switchover operation. It can be seen from the figure that both fans are working in a stable working area, and there is no sudden jump during the adjustment process, so the entire switchover process provides a safe and reliable mine operation.

7 Conclusions

This paper introduces a new non-stop air switchover system of mine main fans based on intelligent control, studies the characteristics of each part of the system, and then establishes the mathematical models, respectively. The improved equalization optimizer algorithm is applied to solve the model.

The novelty and contribution of this paper is that, it establishes a dynamic optimization model on the switchover process of the mine main fans for the first time. Furthermore, it proposes an equilibrium optimizer algorithm improved by chaos mapping and opposition learning machine based on refraction principle to solve the model. The method developed can effectively reduce the change of underground air quantity during the process of fan switchover.

The simulation results show that, the change rate of underground air quantity is always less than 0.4% during the 120 s operation of the fan switchover system, and the operating points of the two main fans are always in the stable working interval without sudden step, which proves the efficiency and safety of the system.

Declaration of conflicting interests

The authors declared no potential conflicts of interest with respect to the research, authorship, and/or publication of this paper.

Data availability

The data that support the findings of this study are available from the corresponding author upon reasonable request.

Funding information

The authors disclosed receipt of the following financial support for the research, authorship, and/or publication of this paper, this work was supported by National Natural Science Foundation of China: Research on prediction method and Application of coal and gas Outburst based on big data (71771111).

Appendix A: Pseudo code of proposed algorithm

1. Initialize the particle's population i=1,.....n
2. Re-initialize particle's population using equation（36）
3. Assign equilibrium candidates' fitness a large number
4. Assign free parameters a1=2;a2=1,GP=0.5;
5. Select four solutions C_{eq1} 、C_{eq2} 、C_{eq3}、C_{eq4}
6. While Iter<Max_Iter
7. For i=1:number of particles(n)
8. Calculate fitness of i^{th} particle
9. If fit(C_i)< fit(C_{eq1})
10. Replace C_{eq1} with C_i and fit(C_{eq1}) with fit(C_i)
11. Elseif If fit(C_i)> fit(C_{eq1}) and fit(C_i)< fit(C_{eq2})
12. Replace C_{eq2} with C_i and fit(C_{eq2}) with fit(C_i)
13. Elseif fit(C_i)> fit(C_{eq1}) and fit(C_i)> fit(C_{eq2}) and fit(C_i)< fit(C_{eq3})
14. Replace C_{eq3} with C_i and fit(C_{eq3}) with fit(C_i)
15. Elseif fit(C_i)> fit(C_{eq1}) and fit(C_i)> fit(C_{eq2}) and fit(C_i)> fit(C_{eq3}) and fit(C_i)< fit(C_{eq4})
16. Replace C_{eq4} with C_i and fit(C_{eq4}) with fit(C_i)
17. End (If)
18. End (For)
19. C_{ave}=(C_{eq1} +C_{eq2} +C_{eq3}+C_{eq4})/4
20. Construct the equilibrium pool C_{eq_pool}=(C_{eq1} 、C_{eq2}、C_{eq3}、C_{eq4} 、C_{ave})
21. Accomplishing memory saving (if Iter>1)
22. Assign t=(1-(Iter/Max_Iter)).^(a2*(Iter/Max_Iter))
23. For i=1:number of paticles(n)
24. Randomly choose one candidate from the equilibrium pool(vector)
25. Generate random vector λ and r
26. Construct F suing equation (29)
27. Construct GCP
28. Construct G_0
29. Construct G
30. Position Update concentrations C
31. Apply OBL mechanism in concentrations C using equation (43)
32. End (For)
33. Return best solution C
34. Iter++
35. End while

References

[1] X. Wu, S. Tian, R. Ma, S. Xu et al., Study on prediction of outburst risk of coal roadway by initial gas emission law of coal body, J. Saf. Sci. Technol. **17**, 116–121 (2021)

[2] X. Liu, J. Liu, M. Qu, Numerical simulation on flame propagation laws of explosion in excavation roadway of high altitude mines, J. Saf. Sci. Technol. **16**, 67–71 (2020)

[3] Q. Zhang, Y. Yao, J. Zhao, Status of mine ventilation technology in China and prospects for intelligent development, Coal Sci. Technol. **48**, 97–103 (2020)

[4] J. Li, Starting way and adjustment method of mine fan as well as relationship, Coal Sci. Technol. **38**, 100–103 (2010)

[5] L. Yu, X. Ma, Z. Ren, S. Yan, Research of switching ventilator control without blowing-out of main ventilator of mine and its implementation, Ind. Mine Autom. Practice **36**, 133–137 (2010)

[6] Z. Wu, Research and application on mine main fans ventilation instability control, China Univ. Mining Technol. Practice **36**, 133–137 (2010)

[7] S. Dong, Design of automatic switchover control system without blowing-out of mine main ventilator based on fuzzy control, Ind. Mine Autom. Practice **41**, 39–43 (2015)

[8] Q. Wang, X. Ma, C. Yang, W. Dai, Modeling and control of mine main fans switchover system, ISA Trans. **85**, 189–199 (2019)

[9] X. Wu, X. Ma, Z. Ren, Study on coal mine main fans automatic switchover aiming at ventilation unceasing and its numerical simulation, in *2010 2nd International Asia Conference on Informatics in Control, Automation and Robotics (CAR 2010)*, IEEE **2**, 227–230 (2010)

[10] Q. Wang, W. Dai, C. Yang, X. Ma, Modeling and analysis of coal mine main fans switchover system, J. China Coal Soc. Practice **43**, 606–614 (2018)

[11] D. Yu, C. Sang, Y. Liu, Z. Cheng, Comparison analysis on air flow testing error of mine main ventilator, Coal Sci. Technol. **46**, 164–168 (2018)

[12] M. Li, H. Ma, Simulation research on airflow measuring method of mine main ventilator, Coal Sci. Technol. **45**, 151–155 (2017)

[13] M. Ye, Y. Yang, Research on graphic digitization and optimization of axial flow fan characteristic curve, Coal Eng. Practice **45**, 110–111+115 (2013)

[14] C. Yin, J. Liu, L. Deng, Characteristic curve of fan fitted with two positive and negative tangent parabolic curve method, J. Liaoning Tech. (Natural Science) Pract. **45**, 110–111+115 (2013)

[15] A. Faramarzi, M. Heidarinejad, B. Stephens et al., Equilibrium optimizer: a novel optimization algorithm, Knowl. Based Syst. **191**, 105190 (2020)

[16] A. Wunnava et al., A novel interdependence based multilevel thresholding technique using adaptive equilibrium optimizer, Eng. Appl. Artif. Intell. **94**, 103836 (2020)

[17] S. Gupta, K. Deep, S. Mirjalili, An efficient equilibrium optimizer with mutation strategy for numerical optimization, Appl. Soft Comput. **96** (2020)

[18] Y. Gao, Y. Zhou, Q. Luo, An efficient binary equilibrium optimizer algorithm for feature selection, IEEE Access **8**, 140936–140963 (2020)

[19] S.K. Dinkar et al., Opposition-based Laplacian equilibrium optimizer with application in image segmentation using multilevel thresholding, Exp. Syst. Appl. **174**, 114766 (2021)

[20] M. Abdel-Basset, R. Mohamed, S. Mirjalili, R.K. Chakrabortty, M.J. Ryan, Solar photovoltaic parameter estimation using an improved equilibrium optimizer, Solar Energy **209**, 694–708 (2020)

[21] M. Abdel-Basset, R. Mohamed, M. Abouhawwash, Balanced multi-objective optimization algorithm using improvement based reference points approach, Swarm Evolut. Comput. **60**, 100791 (2021)

[22] F. Marini, B. Walczak, Particle swarm optimization (PSO). A tutorial, Chemometr. Intell. Laborat. Syst. **149**, 153–165 (2015)

[23] I. Naruei, F. Keynia, Wild horse optimizer: a new meta-heuristic algorithm for solving engineering optimization problems, Eng. Comput. 1–32 (2021)

[24] M. Jain, V. Singh, A. Rani, A novel nature-inspired algorithm for optimization: squirrel search algorithm, Swarm Evolut. Comput. **44**, 148–175 (2019)

[25] S. Mirjalili, Genetic algorithm[M]//Evolutionary algorithms and neural networks (Springer, Cham, 2019), pp. 43–55

[26] Z. Ren, C. Wang, T. Ni, H. Cheng, Research on air volume of reversing without stopping ventilation based on neural network, Coal Technol. **35**, 229–231 (2016)

[27] H.Q. Ge, X.P. Ma, X.Z. Wu et al., Fuzzy PID control of mine main fans switchover aiming at invariant ventilation [C], in *2011 International Conference on Intelligence Science and Information Engineering* (IEEE, 2011), pp. 325–328.

Cite this article as: B.-C. Yu, L.-S. Shao, Optimization of the non-stop switchover system control for the main fans used in mining applications, Mechanics & Industry **23**, 25 (2022)